SCIENTIFIC REPORTS

OPEN

Positive Platinum anomalies at three late Holocene high magnitude volcanic events in Western Hemisphere sediments

Received: 12 March 2018
Accepted: 18 July 2018
Published online: 26 July 2018

Kenneth Barnett Tankersley[1], Nicholas P. Dunning[2], Lewis A. Owen[3], Warren D. Huff[4], Ji Hoon Park[4], Changjoo Kim[2], David L. Lentz[5] & Dominique Sparks-Stokes[1]

Changes in the global atmospheric budget of platinum reportedly correspond to explosive volcanic eruptions. Using inductively coupled plasma mass spectrometry (ICP-MS) elemental analysis we examined eight widely separated stratified sites to evaluate the geographic extent of three late Holocene high magnitude volcanic events. We found characteristic Pt anomalies across the Western Hemisphere dating to the Laki, Iceland (CE 1783–1784), Kuwae, Vanuatu (CE 1452–1453), and Eldgjá, Iceland (CE 934) explosive volcanic eruptions. Pt anomalies in sediments over a broad geographic area indicate distinctive time-correlative atmospheric deposition rates of platinum-rich volcanic ash. These anomalies provide new chronostratigraphic markers for these late Holocene high magnitude volcanic eruptions, which are especially valuable in the Western Hemisphere in strata with limited chronometric control. Pt anomalies provide an important tracer for the age of these volcanic events and ultimately a new chronostratigraphic marker in archaeological, geological, palynological, and paleontological sediments.

In 2011, Soyol-Erdene *et al.*[1] documented atmospheric deposition rates of platinum for the past ~50 years in high summit snow samples collected from two sites in Queen Maud Land, East Antarctica. They sampled snow at 5 cm continuous sequence intervals to a depth of 4 m for Pt concentrations, which were analyzed using inductively coupled plasma mass spectrometry (ICP-MS). Soyol-Erdene *et al.*[1] discovered an anomalously highly elevated Pt concentration that corresponded to the non-sea salt sulfate (nss-SO_4) concentration peak of the 1991–1992 Cerro Hudson volcanic eruption. Their finding demonstrates that Pt can be used as a tracer of the aerosol loading of the atmosphere from a high magnitude volcanic event.

Globally, volcanic Pt emission concentrations are significantly higher than in urban air[2]. The magmatic fractionation of Pt is governed by the volatility of Pt-containing complexes (oxides, hydrogen halides, sulfides) and the physicochemical properties of the magma (temperature, fugacities of relevant chemical species). Pt aerosol layers form in the stratosphere after major volcanic eruptions. The dominant Pt aerosol layer is formed by sulfur dioxide gas, which is converted to droplets of sulfuric acid in the stratosphere over the course of a week to several months after the eruption[3,4]. Winds in the stratosphere spread the Pt aerosols until they practically cover the globe and remain in the stratosphere for about two years. Volcanic ash clouds travel along the same pathways as SO_2 and Pt aerosol particles with a diameter of ~0.1 mm can be widely distributed by prevailing wind patterns[5].

Positive Pt anomalies are concentrations greater than the crustal abundance of 0.5 ppb, and these have been used as reliable tracers for internal geological processes such as tectonic movements, faulting, and hydrothermal activity[6,7]. Pt anomalies are also useful as tracers for the accretion of cosmic dust from comets, meteors, and extra-terrestrial impacts[6–10]. We investigate sediments from eight late Holocene geomorphic/geologic sites that exhibit no or only minimal signs of bioturbation or other natural or cultural disturbance across the Western Hemisphere

[1]Department of Anthropology and Department of Geology, Braunstein Hall, University of Cincinnati, Cincinnati, Ohio, 45220, USA. [2]Department of Geography, Braunstein Hall, University of Cincinnati, Cincinnati, Ohio, 45220, USA. [3]Department of Geology, Geology and Physics Building, University of Cincinnati, Cincinnati, Ohio, 45220, USA. [4]Department of Geography Education, Kongju National University, Chungcheongnam-do, 32588, South Korea. [5]Department of Biology, Rieveschl Hall, University of Cincinnati, Cincinnati, Ohio, 45221, USA. Correspondence and requests for materials should be addressed to K.B.T. (email: tankerkh@uc.edu)

where hot springs, faults, and chondrite-rich sediments containing magnetic microspherules and microtektites were absent. These sites allow us to test the occurrence of Pt anomalies at the timing of three high-magnitude late Holocene volcanic events (Supplementary Information). Unlike varved sediments in glacial lakes, undisturbed, well-stratified, and dated geomorphic/geologic sites have a wider geographic distribution and offer more opportunities to examine the occurrence of positive Pt anomalies.

While not all explosive eruptions with a volcanic explosivity index (VEI) $\geq$5 result in global distributions of tephra, there is causal link between high-magnitude volcanic events and late Holocene climatic change, the most profound of which in terms of human impact is known as the Little Ice Age[11]. Northern latitude tephras tend to remain in the northern hemisphere and tropical latitude eruptions such as Kuwae have global distributions. High-magnitude volcanic activity produces ash and SO_2, which reaches the stratosphere creating a pan-global ash cloud obstructing solar radiation and results in global cooling. Theoretically, a long-term feedback loop is created when cooled ocean waters and an increase in sea ice result in unusually cold summers[12]. Volcanic ash and SO_2 from the CE 1452–1453 eruption of the Kuwae volcano in the Republic of Vanuatu and the CE 1783–1784 eruption of the Laki volcano system have been posited as significant contributing factors in the global cooling of the Little Ice Age[11,13]. The ~CE 934 eruption of the Eldgjá volcano in Iceland occurred at the beginning of a warm climatic period in the North Atlantic known as the Medieval Climate Optimum[14]. A climatic warming period may result when significant amounts of volcanic carbon dioxide, a greenhouse gas, are produced.

Kuwae is a submarine volcanic caldera located between the Epi and Tongoa islands. Sometime between late CE 1452 and early CE 1453, Kuwae produced ~32–39 km^3 of magma and a stratospheric injection of ~175–700 Mt of H_2SO_4[14]. Kuwae's cataclysmic eruption (VEI 7) is considered one of the most explosive volcanic events of the Holocene. Evidence of the Kuwae volcanic eruption is represented in 13 Greenland and 20 Antarctic ice cores as an anomalous sulfate spike[15]. The high magnitude of the Kuwae eruption is based on ~93 kg SO_4/km^3 in Antarctica ice cores and ~45 kg SO_4/km^3 in the Greenland ice cores[16].

The Laki volcanic system is located in southern Iceland and includes the Lakagígar volcanic vent or fissure, the Grímsvötn caldera, and the subglacial Thordarhyrna volcano. Explosive eruptions (VEI 6) in the Laki volcanic system occurred between June 1783 and February 1784[16]. During this time, the Laki system produced a convective column of ~120 Mt of SO_2 into the stratosphere and erupted ~14 km^3 of basalt lava[16]. The large volume of volcanic ash, water vapor, and reflected solar radiation and absorbed terrestrial radiation resulted in one the longest and coldest drops in historically recorded global temperatures[17].

Eldgjá is part of the southern Iceland Laki volcanic system, and includes the Katla volcano[18]. Eldgjá's colossal eruption (VEI 6) originated from a ~200-m deep rift at ~CE 934[18–20]. The eruption produced ~219 Mt of SO_2, a ~6 km^3 terrestrial ash fall, and erupted ~19.6 km^3 of basaltic lava. These are conservative estimations because they do not include ash fall in the ocean or portions of lava flows, which are now covered by late Holocene sediments. Eldgjá was the largest volcanic eruption historically recorded and it produced the largest lava flow during the late Holocene[19]. Written records from Iceland, Western Europe, the Middle East, and Asia document global cooling, famine, and epidemics for ~9 years following the eruption[20].

We hypothesized that Pt anomalies resulting from three late Holocene high magnitude volcanic events should be present in contemporary sediments across the Western Hemisphere given that Soyol-Erdene *et al.*[1] found a Pt anomaly in Antarctic snow samples that was associated with a paroxysmic volcanic eruption. Our investigation aims to: a) determine if Pt anomalies from the Laki (CE 1783–1784), Kuwae (CE 1452–1453), and Eldgjá (CE 934) volcanic events might be present in sediments: and b) ascertain if Pt anomalies can be used to distinguish certain high-magnitude volcanic events (VEI $\geq$ 5) at locations with less precise chronostratigraphic control.

We tested our hypothesis that late Holocene high-magnitude volcanic events would reveal Pt anomalies in sediments obtained from eight well-stratified and chronometrically dated sites across the Western Hemisphere. These sites include: the Temple Reservoir tank at the Maya city of Tikal in the Petén District of northern Guatemala; Nonsuch Bay on the island of Antigua in the West Indies region of the Caribbean; an Ancestral Puebloan canal in Chaco Canyon, New Mexico; the Albert Porter Pueblo and Wallace Ruin, two Ancestral Puebloan Great Houses in southwestern Colorado; Big Bone Lick, Kentucky, a historic contact Fort Ancient bison kill site and a critical geologic site in the historical development of North American Quaternary science and vertebrate paleontology; a sinkhole at Serpent Mound, a 411 m-long earthwork on a karst plateau in southern Ohio; and Wynema, a historic contact Fort Ancient village site in southwestern Ohio (Fig. 1 and Supplementary Information).

We postulated that if these stratified late Holocene sites contained sediments that were deposited at the time of the Laki (CE 1783–1784), Kuwae (CE 1452–1453), and Eldgjá (CE 934) volcanic events, then we should expect to find Pt anomalies. The sediment sample sites have been well-described elsewhere and are also presented in the Supplementary Information. While the sites varied greatly in their age range and geologic setting, all of the sample sites dated to one or more of the late Holocene volcanic events and the sediments were deposited in low energy environments. Sediment samples from the Temple Reservoir tank consisted of aggrading clays[21,22]. The Nonsuch Bay sediment samples consisted of well stratified hemic and sapric organic clays[23]. The American Southwestern samples were poorly consolidated clay, silt, and coarse to medium sand and sandy silty alluvium from Chaco Canyon and a fine-textured silt and fine to medium sandy alluvium overlying an iron-stained clayey silt and fine sandy loess at the Albert Porter Pueblo and Wallace Ruin[24–26]. The Midwestern samples from Big Bone Lick and the Wynema site consisted of a deep and uniformly finely laminated silty alluvium[27]. The Serpent Mound samples consisted of well-stratified silt, silty clay, and clay karst sinkhole deposits[28].

Results and Discussion

The ages of the sediments at our six late Holocene temperate latitude (36–39°N) sample sites in North America (Albert Porter Pueblo, Colorado; Big Bone Lick, Kentucky; Chaco Canyon, New Mexico; Serpent Mound, Ohio, Wallace Ruin, Colorado; Wynema, Ohio; Figs 2 and 3) and our two tropical latitude (17°N) sites (Nonsuch Bay, Antigua; Temple Reservoir tank Tikal, Guatemala; Fig. 3) are based on multiple dating techniques including

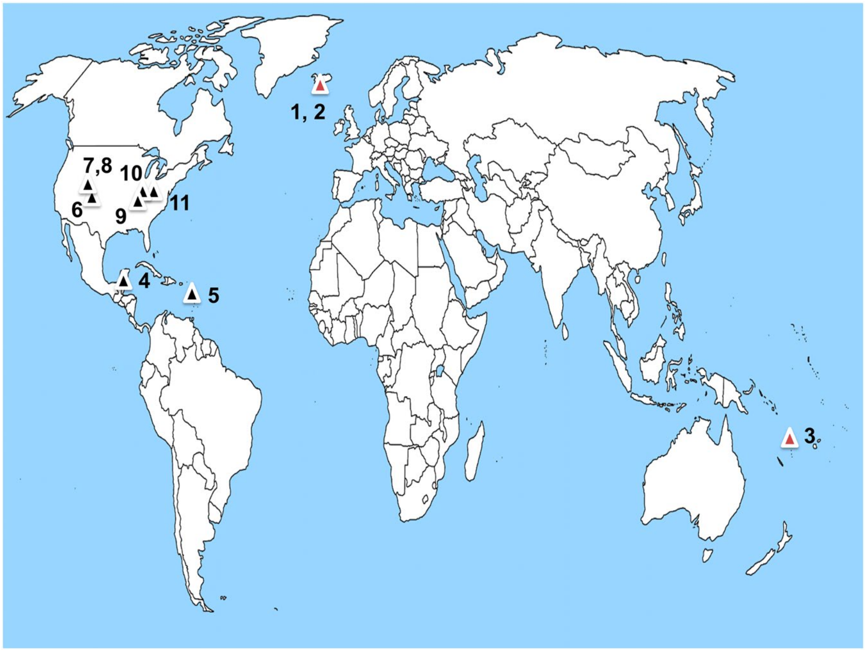

Figure 1. Map showing volcanic centers (red triangles) for late Holocene high-magnitude eruptions (black triangles) for Laki volcanic system (#1), Eldgjá volcanic fissure (#2) and Kuwae volcano (#3). Study sites for platinum (black triangles) include: Temple Reservoir tank, Tikal, Guatemala (#4); Nonsuch Bay, Antigua (#5); Chaco Canyon, New Mexico (#6); Albert Porter Pueblo, Colorado (#7); Wallace Ruin, Colorado (#8); Big Bone Lick, Kentucky (#9); Wynema, Ohio (#10); and Great Serpent Mound, Ohio (#11).

AMS radiocarbon, optically stimulated luminescence (OSL), dendrochronology, tephra, and artifact typologies. Our analyses identified Pt anomalies at each site in dated strata, which correlated with one or more late Holocene high-magnitude volcanic event.

Our reported results from 39–17° N latitudes and 108–61° W longitudes provide evidence of Pt enrichment in sediments that date to the timing of the high magnitude Laki, Iceland (CE 1783–1784), Kuwae, Vanuatu (CE 1452–1453), and Eldgjá, Iceland (CE 934) volcanic eruptions (Figs 2 and 3; Supplementary Information). Pt anomalies averaged 2.3 ppb at our study sites (range: 1.1 to 5.3 ppb) compared to background abundances (0.0–0.5 ppb) above and below the late Holocene anomalies for these high magnitude volcanic eruptions. They are 5x higher than crustal abundance of 0.5 ppb.

A Pt anomaly was detected in sediments that date to the time of the Laki volcanic system eruption at seven of the sites we sampled (Albert Porter Pueblo, Big Bone Lick, Chaco Canyon, Nonsuch Bay, Serpent Mound, Wallace Ruin, Wynema) and averaged 2.4 ppb and ranged from 1.8 to 2.9 ppb. Another Pt anomaly was found in sediments that date to the time of the Kuwae volcanic eruption at five of the sites we sampled (Albert Porter Pueblo, Big Bone Lick, Nonsuch Bay, Serpent Mound, Wynema) and averaged 2.9 ppb and ranged from 0.6 to 5.2 ppb. A Pt anomaly was also recovered in sediments that date to the time of the Eldgjá volcanic eruption at four of the sites we sampled (Albert Porter Pueblo, Serpent Mound, Temple Reservoir, Wynema) and averaged 2.2 ppb and ranged from 1.1 to 5.1 ppb.

Pt anomalies, which date to the timing of all three of the high-magnitude late Holocene volcanic eruptions, were found in sediment samples from the Albert Porter Pueblo, Serpent Mound, and Wynema sites. Pt anomalies, which correspond to the age of the eruption of the Laki volcanic system, were found in sediment samples from seven of the sites sampled (Albert Porter Pueblo, Big Bone Lick, Chaco Canyon, Nonsuch Bay, Serpent Mound, Wynema). The Pt concentrations between the sites have a relatively small sample variance (0.2), that is, the variation of Pt values. The recent age (CE 1783–1784) of the Laki volcanic event may be the reason for the inter-site consistency of the Pt concentration. That is, it is less likely that post-depositional processes have altered the original Pt content of younger sediments.

Measured concentrations of Pt in late Holocene sediments likely depend upon the distance between the sample site location and the volcano, eruption strength, ash composition, and distribution area of the ejecta. Pt-rich ash, which reached the stratosphere would have had the broadest geographic distribution[1]. Depletion of Pt concentrations at some of the sample sites may have been the result of the size of the site catchment basin, discontinuous deposition, and/or post-depositional erosional processes[7]. Nonetheless, the average Pt anomalies described here for temperate and tropical latitude sites in the Western Hemisphere are relatively consistent in magnitude with regard to the VEI magnitudes of the Laki (mean 2.4 ppb Pt, VEI 6), Kuwae (mean 2.9 ppb Pt, VEI 7), and Eldgjá (mean 2.2 ppb Pt, VEI 6) events. Consequently, Pt concentrations provide an important new tracer for the age of these events and ultimately new chronostratigraphic markers. The widespread distribution of Pt in late Holocene sediments further illustrates the global impact of high magnitude volcanic eruptions, and possibly their role in periods of climatic change such as those experienced during the Little Ice Age.

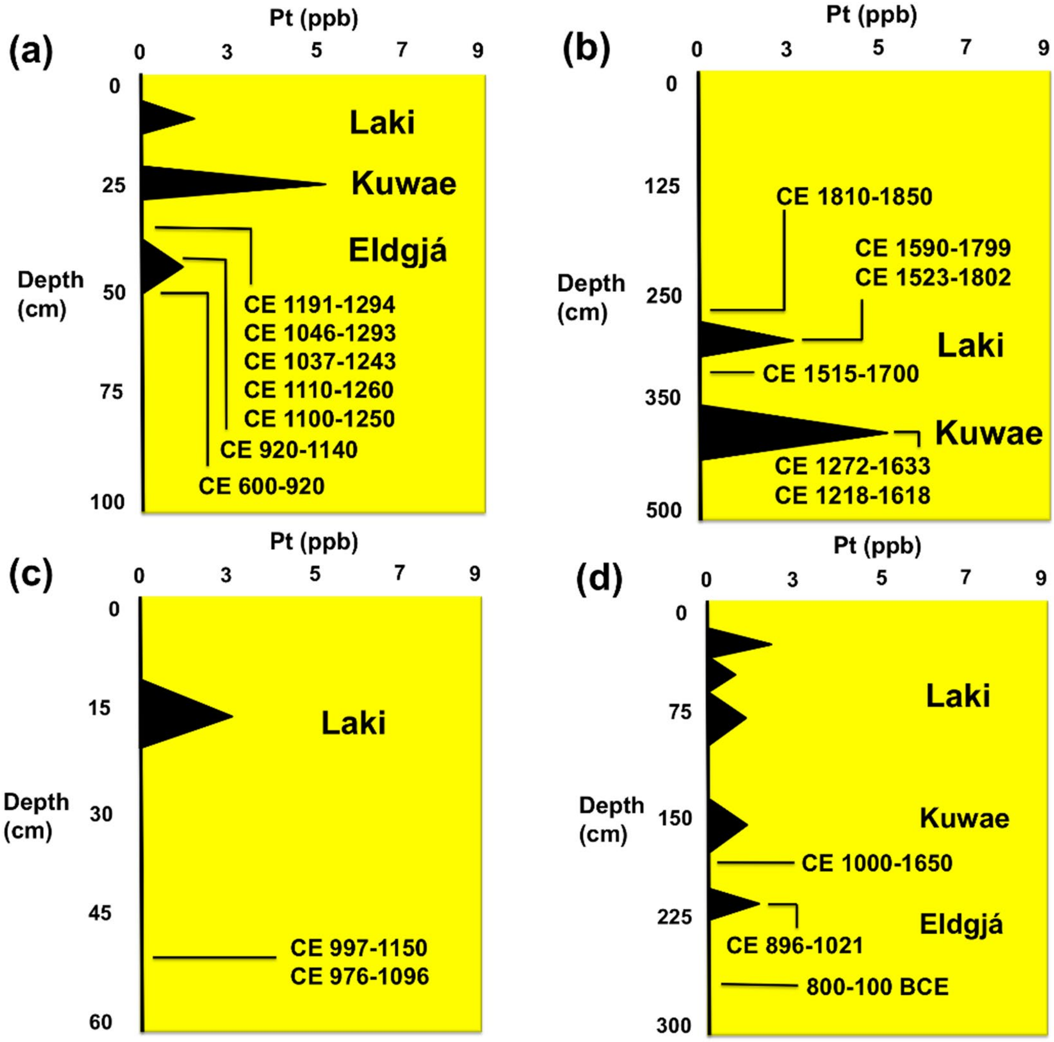

Figure 2. Site graphs for northern latitude (36–39^0) study sites showing abundance of Pt in ppb (±0.1 ppb), depth, and AMS radiocarbon ages (calibrated years CE with 2 σ uncertainty): (**a**) Albert Porter Pueblo, Colorado; (**b**) Big Bone Lick, Kentucky; (**c**) Chaco Canyon, New Mexico; (**d**) Serpent Mound, Ohio. See Supplementary Information for additional chronostratigraphic details. Zero values represent below detection levels.

Conclusion

Pt anomalies occur in sediments from geographically widely separated sites across the Western Hemisphere, which date to the Laki (CE 1783–1784), Kuwae (CE 1452-1453), and Eldgjá (CE 934) volcanic eruptions. Despite inter-site variances, which likely resulted from post-depositional erosional processes, Pt anomalies provide an effective tracer for certain late Holocene high-magnitude (VEI ≥ 6) volcanic events and ultimately provide three new chronostratigraphic markers on archaeological, geological, palynological, and paleontological sites. The concentrations of Pt from well-dated and well-stratified late Holocene sites provide an opportunity for more vigorous evaluations of the impact of high magnitude volcanic eruptions on climate change and society.

Methods

Sediment samples were collected from each site in continuous manner by depth. Supplementary Information provides detailed chronostratigraphic information for each of the sites sampled and detailed data are provided for each site related to stratigraphy, age, sampling provenience, and cultural components in Tables 1–17 and Figs 1–3.

Selected aliquots of sediment from late Holocene sites were transferred to pre-weighed digestion vessels. All solutions were prepared with certified trace-metal grade HNO_3 (67–70% w/w) and HCl (36% w/w) and ultra-pure (18MΩ) water. Sediment aliquots were homogenized and digested with Aqua Regia (3:1 HCl:HNO_3 mol/mol) in Savillex PFA containers and heated at 90 °C for 1 hour on a heating block. After cooling, the solutions were then diluted with 18 MΩ water and analyzed by ICP-MS[29]. The certified reference material (SARM-7, SACCRM) was digested using the same procedure as a means of corroboration. The value of the certified reference material (SARM-7, SACCRM) was 3.74 ± 0.05 ppm and the measured value was 4.27 ± 0.13 ppm.

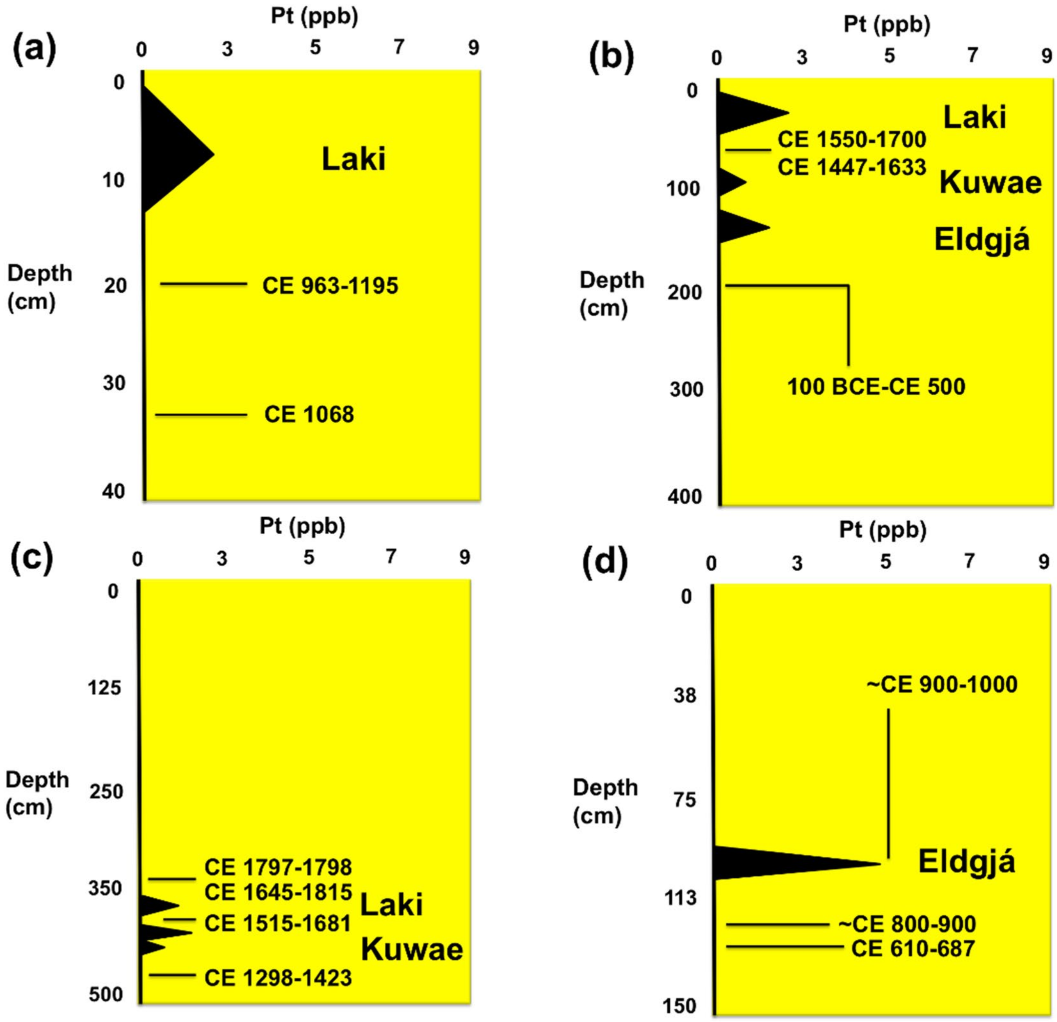

Figure 3. Site graphs for northern latitude (36–39^0) and tropical latitude (17^0) study sites showing abundance of Pt in ppb (±0.1 ppb), depth, and radiocarbon ages (calibrated years CE with 2 σ uncertainty); (**a**) Wallace Ruin, Colorado; (**b**) Wynema, Ohio. (**c**) Nonsuch Bay, Antigua, (**d**) Temple Reservoir Tank, Tikal, Guatemala. See Supplementary Information for additional chronostratigraphic details. Zero values represent below detection levels.

ICP-MS analyses were completed on a Thermo Scientific X Series II instrument. A peristaltic pump using a Cetac ASX 520 auto-sampler pumped sample solutions. The internal standard was added in-line using a Trident Internal Standard Kit. The sample was introduced into the plasma using a MicroMist EzyFit nebulizer, which reduced oxide formation with a high total dissolved solids tolerance, and reduced the sample uptake rates. The cyclonic spray chamber was kept at 3 °C, minimizing oxide formation. Ion lens voltages, nebulizer flow, and stage positioning were optimized every 24 hours using a tuning solution to maximize the ion signal and stability and minimize oxide levels (CeO^+/Ce^+) and doubly charged ions (Ba^{2+}/Ba^+). A calibration check of the standards was analyzed following initial calibration, at the end of the sample run, and after every 12 samples.

Data Availability. All data generated or analyzed during this study are included in this published article (and its Supplementary Information files).

References

1. Soyol-Erdene, T., Huh, Y., Hong, S. & Hur, S. D. A 50-Year Record of Platinum, Iridium, and Rhodium in Antarctic Snow: Volcanic and Anthropogenic Sources. *Environmental Science and Technology* **45**, 5929–5935 (2011).
2. Moune, S., Faure, F., Gauthier, P. J. & Sims, K. W. W. Pele's hairs and tears: natural probe of volcanic plume. *Journal of Volcanology and Geothermal Research* **164**, 244–253 (2007).
3. Giammanco, S., Sims, K. W. W. & Neri, M. Measurements of ^{220}Rn and ^{222}Rn and CO_2 emissions in soil and fumarole gases on Mt. Etna volcano (Italy): Implications for gas transport and shallow ground fracture. *Geochemistry, Geophysics, Geosystems* **8**(10), 1644 (2007).
4. Villemant, B., Salaün, A. & Staudacher, T. Evidence for a homogeneous primary magma at Piton de la Fournaise (La Réunion): A geochemical study of matrix glass, melt inclusions and Pélé's hairs of the 1998–2008 eruptive activity. *Journal of Volcanology and Geothermal Research* **184**, 79–92 (2009).

5. Stohl, A. *et al*. Determination of time- and height-resolved volcanic ash emissions and their use for quantitative ash dispersion modeling: the 2010 Eyjafjallajökull eruption. *Atmospheric Chemistry and Physics* **11**, 4333–4351 (2011).
6. Lorand, J. P., Luguet, A. & Alard, O. Platinum-group elements: a new set of key tracers for the Earth's interior. *Elements* **4**, 247–252 (2008).
7. Moore, C. R. *et al*. Widespread platinum anomaly documented at the Younger Dryas onset in North American sedimentary sequences. *Scientific Reports* **7**, (44031),https://doi.org/10.1038/srep44031 (2017).
8. Peucker-Ehrenbrink, B. & Ravizza, G. The effects of sampling artifacts on cosmic dust flux estimates: a reevaluation of nonvolatile tracers (Os, Ir). *Geochim. Cosmochim. Acta* **64**(11), 1965–1970 (2000).
9. Gabrielli, P. *et al*. Meteoric smoke fallout over the Holocene epoch revealed by iridium and platinum in Greenland ice. *Nature* **432**, 1011–1014 (2004).
10. Karner, D. B. *et al*. Extraterrestrial accretion from the GISP2 ice core. *Geochim. Cosmochim. Acta* **67**(4), 751–763 (2003).
11. Miller, G. H. *et al*. Abrupt onset of the Little Ice Age triggered by volcanism and sustained by sea-ice/ocean feedbacks. *Geophysical Research Letters* **39**(31), L02708, https://doi.org/10.1029/2011GL050168 (2012).
12. Robock, A. The Little Ice Age: Northern Hemisphere Average Observations and Model Calculations. *Science* **206**(4425), 1402–4 (1979).
13. Jonathan, C. *Climate change: biological and human aspects*. Cambridge University Press (2007).
14. Crowley, T. J. & Lowery, T. S. How Warm Was the Medieval Warm Period? *AMBIO: A Journal of the Human Environment* **29**, 51 (2000).
15. Gao, C. *et al*. The 1452 or 1453 AD Kuwae eruption signal derived from multiple ice core records: Greatest volcanic sulfate event of the past 700 years. *Journal of Geophysical Research* **111**(D12), D12107 (2006).
16. Gudmundsson, M. T. & Högnadóttir, T. Volcanic systems and calderas in the Vatnajökull region, central Iceland: Constraints on crustal structure from gravity data. *Journal of Geodynamics.* **43**(1), 153–169 (January 2007).
17. Robock, A. Volcanic eruptions and climate. *Reviews of geophysics* **38**(2), 191–219 (2000).
18. Simkin, T. & Siebert, L. *Volcanoes of the World*. (Geoscience Press, Tucson, Arizona, 1994).
19. Árni Hjartarson, A. Víðáttumestu hraun Íslands. *Náttúrufræðingurinn* **81**, 37–49 (2011).
20. Stothers, R. B. Far reach of the tenth century Eldgjá eruption, Iceland. *Climatic Change* **39**, 715–726 (1998).
21. Dunning, N. P., *et al*. Life on the Edge: Tikal in a BajoLandscape. Lentz, D., N. Dunning, and V. Scarborough (eds). *Tikal: Paleoecology of an Ancient Maya City*, Pp. 95–123, Cambridge University Press (2015).
22. Scarborough, V., *et al*. Water and Sustainable Land Use at the Ancient Tropical City of Tikal, Guatemala. *Proceedings of the National Academy of Sciences* 12408–12413 (2012).
23. Wells, E. C. *et al*. Plantation Soilscapes: Initial and Cumulative Impacts of Colonial Agriculture in Antigua, West Indies. *Environmental Archaeology* **22**, 23–35 (2018).
24. Tankersley, K. B., Huff, W. D., Dunning, N. P., Owen, L. A. & Scarborough, V. L. Volcanic minerals in Chaco Canyon, New Mexico and their archaeological significance. *Journal of Archaeological Science: Reports* **17**, 404–421 (2018).
25. Ryan, S. C. *The archaeology of Albert Porter Pueblo (Site 5MT123): excavations at a Great House community center in southwestern Colorado*. (Crow Canyon Archaeological Center, Cortez, Colorado, 2015).
26. Bradley, B. Excavations at Wallace Ruin (5MT6970) Montezuma County, Colorado 1998–2010 University of Exeter (2010).
27. Tankersley, K. B. *et al*. Quaternary chronostratigraphy and stable isotope paleoecology of Big Bone Lick, Kentucky, USA. *Quaternary Research* **83**, 479–487 (2015).
28. Dalby, T. S. *Geological Aspects of Key Archaeological Sites in Northern Kentucky andSouthern Ohio*, edited by Timothy S. Ohio Geological Survey, Columbus, Ohio (2007).
29. Cicchella, D., De Vivo, B. & Lima, A. Palladium and platinum concentrations in soils from the Napoli metropolitan area, Italy: possible effects of catalytic exhausts. *Science of the Total Environment* **308**, 121–131 (2003).

Acknowledgements

This research was made possible with support from the Charles Phelps Taft Foundation, the Court Family Foundation, and the University of Cincinnati Research Council. We are especially grateful to Mark Varian, Bruce Bradley, Bradley Lepper, Kathy Loftus, Peter Siegel, Vernon Scarborough, the Antigua and Tikal research teams, the Crow Canyon Archaeological Center, Chaco Culture National Historical Park, National Park Service, the Navajo Nation, members of the American Indian Advisory Council, and the Center for Applied Isotope Studies.

Author Contributions

K.B.T. conceived the project. K.B.T., N.P.D., L.A.O., W.D.H. wrote most of the manuscript. K.B.T., N.P.D., D.L.L., L.A.O., J.H.P., C.K. directed most of the fieldwork and D.S.S contributed laboratory data. L.A.O. did the OSL dating.

Additional Information

Supplementary information accompanies this paper at https://doi.org/10.1038/s41598-018-29741-8.

Competing Interests: The authors declare no competing interests.

Supplementary Information: Site Data, Pt Aerosols, and Tephra Volume

Positive Platinum anomalies at three late Holocene high magnitude volcanic events in Western Hemisphere sediments

Kenneth Barnett Tankersley*[1,2], Nicholas P. Dunning[3], Lewis A. Owen[2], Warren D. Huff[2], Ji Hoon Park[4], Changjoo Kim[3], David L. Lentz[5], Dominique Sparks-Stokes[1].

[*1]Department of Anthropology, University of Cincinnati, Cincinnati, Ohio, 45221, USA.
[2]Department of Geology, University of Cincinnati, Cincinnati, Ohio, 45221, USA.
[3]Department of Geography, University of Cincinnati, Cincinnati, Ohio, 45221, USA.
[4]Department of Geography Education, Kongju National University, Chungcheongnam-do, 32588, Korea.

Table 1. Site Pt peak data summary[a,b].

Sample Site	**Laki (Pt ppb)**	**Kuwae (Pt ppb)**	**Eldgjá (Pt ppb)**
Albert Porter Pueblo, Colorado	1.8	5.3	1.4
Big Bone Lick, Kentucky	2.3	4.7	nd
Chaco Canyon, New Mexico	2.8	nd	nd
Nonsuch Bay, Antigua	2.6	2.6	nd
Serpent Mound, Ohio	1.8	1.1	1.2
Temple Reservoir Tank, Guatemala	nd	nd	5.1
Wallace Ruin, Colorado	2.5	nd	nd
Wynema, Ohio	2.9	0.6	1.1
Range	1.8–2.9	0.6–5.3	1.1–5.1
Mean	2.4	2.9	2.2

a. nd = no data.
b. SARM-7 certified value was 3.74 ± 0.05 ppm and the measured value was 4.27 ± 0.13 ppm.

Antigua

Nonsuch Bay

Nonsuch Bay is a prominent embayment on the eastern side of the island of Antigua, West Indies (Figure 1). Core NS07-2 was collected as part of a multi-island paleoecology project that examined the pattern of human migration and environmental disturbance in the Lesser Antilles[1,2]. The 456-cm-long core was retrieved with a modified Livingston piston corer in a mangrove-dominated estuary where Ayres Creek discharges into the bay. The stratigraphy of the core exhibited great integrity with only minimal signs of bioturbation or other disturbance (e.g., a small amount of mangrove root penetration between 390 and 405 cm. depth). The portions of the core discussed in this article are illustrated in Figure 1; the entire core is described in detail elsewhere.[2] A radiocarbon age of 580 $\pm$ 35 BP (calibrated to 1300–1420 CE; all radiocarbon ages in this supplement are calibrated using CALIB 7.1 and the IntCal13 calibration) was obtained from "sapric clay" (clay with between 5-10% sapric organic matter) sediment from 445 cm (Table 2, Figure 1). Data from the core and from survey in the contributing watershed indicates catastrophic soil erosion associated with Colonial era sugarcane cultivation is responsible for most of the sediment in the estuary[3]. The samples reported here are from between depths of 349 and 439 cm in the core (Table 3). Most of the core in this section consists of clay with a high organic matter content. Lenses of volcanic ash at 351−348 cm and 362−360 cm likely correspond to the CE 1797−1798 eruption of La Grande Soufrière on the island of Guadeloupe which is reported to have resulted in significant ash fall on Antigua. The samples reported here straddle the lower and middle of three pollen zones identified in the NS07-02 core, that is, the transition from the pre-Columbian and earliest Colonial eras to the era of peak Colonial plantation agriculture with its associated deforestation and soil erosion.[2] These pollen data are consistent with the radiocarbon-based chronology.

Figure 1. A cross-section of the Nonsuch Bay, Antiqua core and site location.

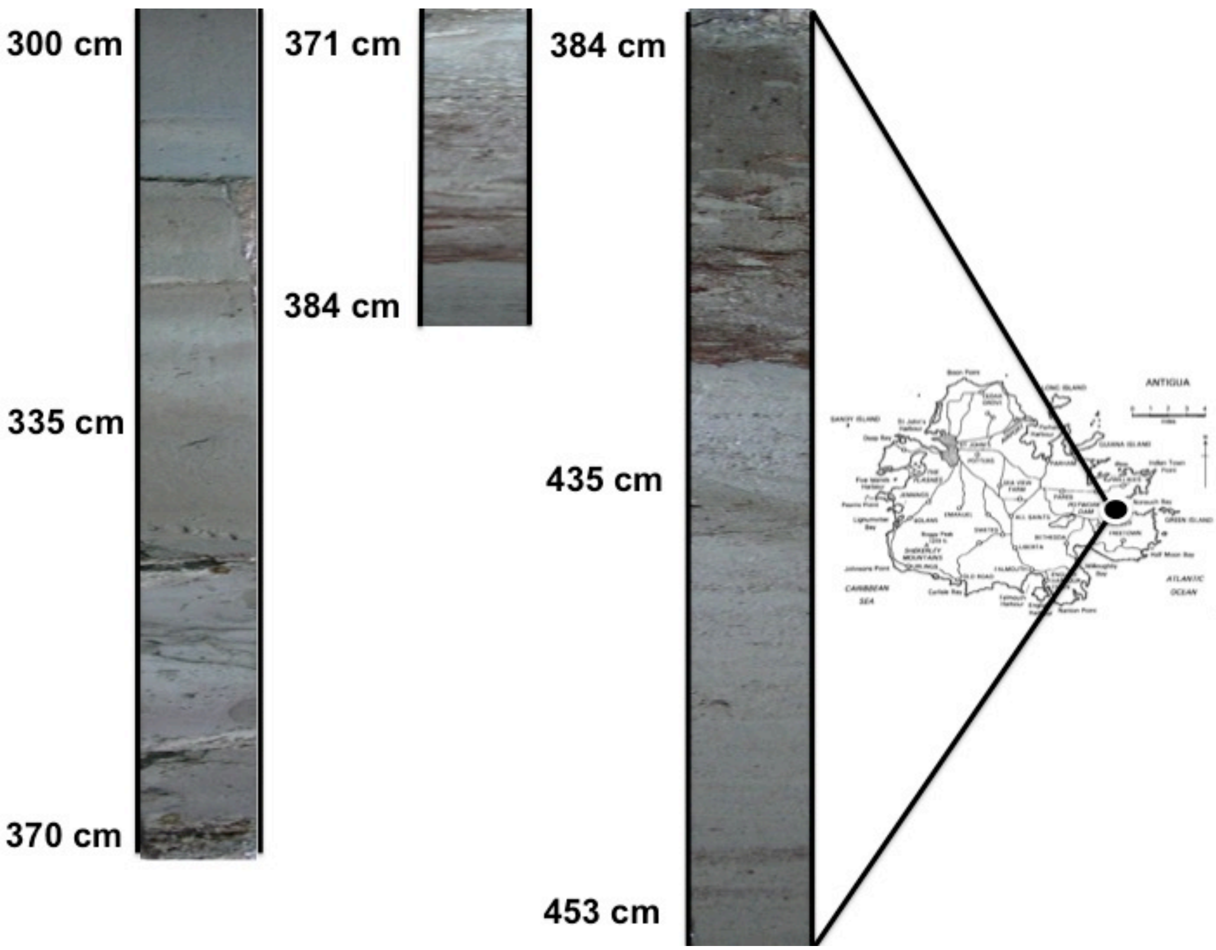

Table 2. Radiocarbon and tephra ages for Nonsuch Bay, Antiqua.

Sample	Lab #	^{14}C age yr BP	Cal age (2 σ)[a]	Probability
Tephra			CE 1797−1798	
Organic Matter	AA82476	191 ± 38	CE 1645−1697	0.240
			CE 1724−1815	0.531
			CE 1834−1878	0.059
			CE 1916−1950	0.169
Organic Matter	AA82475	254 ± 36	CE 1515−1598	0.277
			CE 1617−1681	0.495
			CE 1739−1745	0.005
			CE 1762−1802	0.187
			CE 1937−1950	0.035
Organic Matter	AA77643	577 ± 37	CE 1298−1371	0.641
			CE 1379−1423	0.359

a. CALIB 7.1 and the IntCal13 Calibration.

Figure 2. Bayesian adjustments of the radiocarbon ages using OXCAL to give the full range of possible ages for Nonsuch Bay, Antiqua.

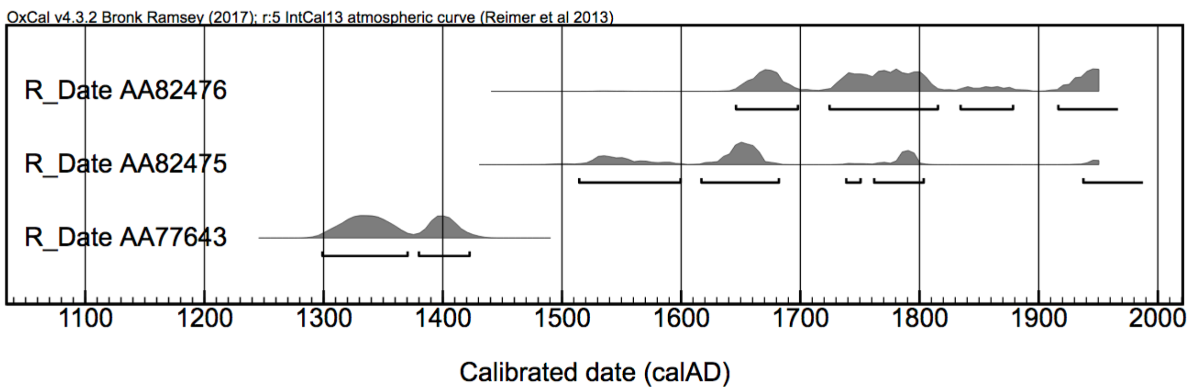

Table 3. Chronostratigraphy and Pt values for Nonsuch Bay, Antiqua.

Depth (m)	Composition	Munsell Soil Color	Age	Pt (ppb)[a]
3.51-3.60	Banded Sapric clay	Gley 10Y 5/1	CE 1797−1798	nd
3.49	Sapric clay	Gley 10Y5/1	CE 1645−1815	nd
3.90	Hemic peat	Gley 10Y2.5/1		2.6
3.98	Hemic peat	Gley 10Y2.5/1	CE 1515−1681	nd
4.20	Sapric clay	Gley 10Y3/1		2.6
4.39	Sapric clay	Gley 10Y3/1		1.8
4.45	Sapric clay	Gley 10Y3/1	CE 1298−1423	nd

a. nd = no data

Guatemala

Temple Reservoir Tank, Tikal,

The Temple Reservoir Tank is located in the heart of an area of monumental architecture in "downtown" Tikal, an ancient Maya city in the Peten District of Guatemala (Figure 3). This feature lies above the much larger Temple Reservoir proper. Originally thought to be a silting tank to protect water quality in the Temple Reservoir, excavations in 2009 revealed that the tank seems to have been designed to collect water from a now plugged natural spring[4,5]. Excavations and coring in the tank indicated that it was periodically dredged, but seems to have steadily accumulated clayey sediment from the Seventh century CE onward (Table 4). Operation 7A was a 1 x 1 m excavation that penetrated to sterile substrate at a depth of about 2.2 m. Strata revealed within the profile showed little disturbance from either bioturbation or argilloturbation (clay heaving), both of which sometimes disturb strata in the Maya Lowlands. The charcoal sample reported here was collected from the pit wall at a depth of 130 cm; the analyzed sediment sample was collected from the pit wall at a depth of 100 cm (Table 5), which should correspond to the period between CE 900 and 1100. Although abundant ceramic sherds were recovered in Op. 7A, almost all were too weathered for chronological identification (typical of reservoir sherds). Between a depth of 125 and 150 cm, sherds were extremely abundant and seem to correspond to the Late Classic period (CE 600-800), consistent with the radiocarbon date. Between a depth of 125 and 100 cm, sherds diminished dramatically in number and those identifiable were a mixed lot of Classic Period types, consistent with Terminal Classic and post-abandonment deposits (i.e., consistent with a 9th century chronological date). Only a handful of unidentifiable sherds were recovered between 85 and 100 cm (consistent with post-abandonment deposits; i.e., a 10th century CE date)[6,7].

Figure 3. Profile of the Tikal, Guatemala excavation and site location.

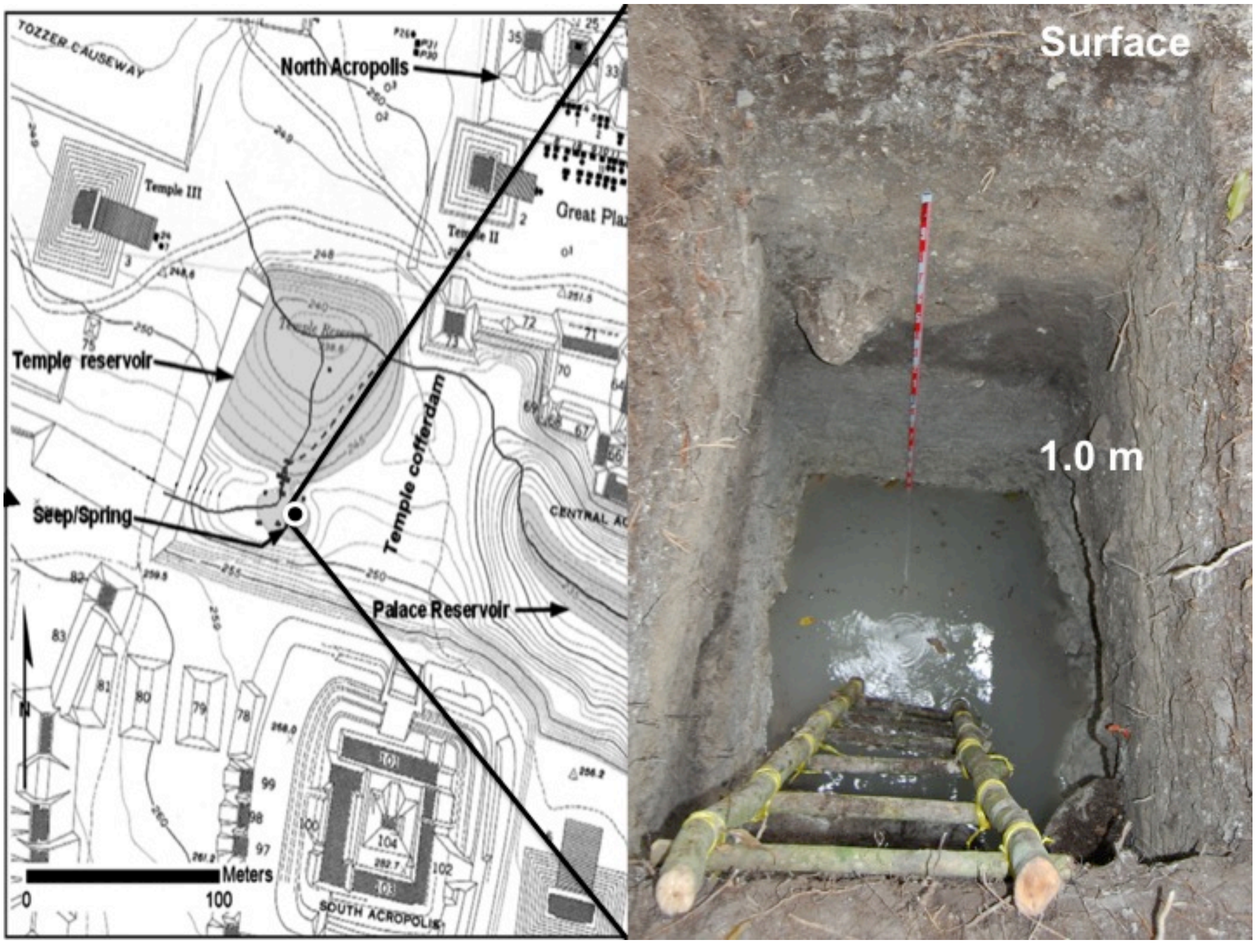

Table 4. Radiocarbon and ceramic typological ages for Temple Reservoir Tank, Tikal.

Sample	**Lab #**	**^{14}C age yr BP**	**Cal age (2 σ)[a]**	**Probability**
Post-abandonment Refuse			~CE 900-1000	
Terminal Classic Mixed Ceramic Deposit			~CE 800−900	
Late Classic ceramics			~CE 600-800	
Wood Charcoal	Beta 298985	1370 ± 30	CE 610−687	1.000

A. CALIB 7.1 and the IntCal13 Calibration.

Table 5. Chronostratigraphy and Pt values for Temple Reservoir Tank, Tikal.

Depth (m)	**Texture**	**Munsell Soil Color**	**Age**	**Pt (ppb)[a]**
1.0	Silty clay	7.5YR6/1	~CE 900-1000	5.1
1.25	Silty clay	7.5YR7/1	~CE 800−900	
1.3	Silty clay	7.5YR7/1	CE 610−687	Nd

a. nd = no data.

USA

Albert Porter Pueblo, Colorado

Albert Porter Pueblo is an Ancestral Publoan village located on a mesa top between Sandstone and Woods Canyons in southwestern Colorado (Figure 4). The site includes Chacoan masonry, 28 multistory rooms, 26 kivas, 6 pit structures, and 54 midden deposits. Dendrochronology samples obtained from the Albert Porter Pueblo span from ~CE 860−1260 and cutting ages for the wood suggest that the site was occupied continuously from ~ CE 1110−1260[8]. Radiocarbon ages are consistent with the dendrochronology (Table 6, Figure 5). The oldest ceramic artifacts from the Albert Porter Pueblo date to the Basketmaker III and Pueblo I cultural periods (~ CE 600–920). The midden deposits are dominated by ceramic artifacts, which date to the Pueblo II and Pueblo III (~ CE 920–1140) cultural periods with the greatest concentration of pottery dating to ~ CE 1100–1250[8]. Sediment samples were obtained from a solid sediment core extracted from the open plaza of the pueblo. Natural stratigraphy was defined on the basis of soil texture and color (Table 7). Sediment samples were collected from the open-air plaza portion of the site with intact stratigraphy. There was no evidence of bioturbation or other natural or cultural disturbances. The stratigraphy discussed in this article is illustrated in Figure 5 and the entire site is described in detail elsewhere[8].

Figure 4. Profile of the Albert Porter Pueblo, Colorado excavation and site location.

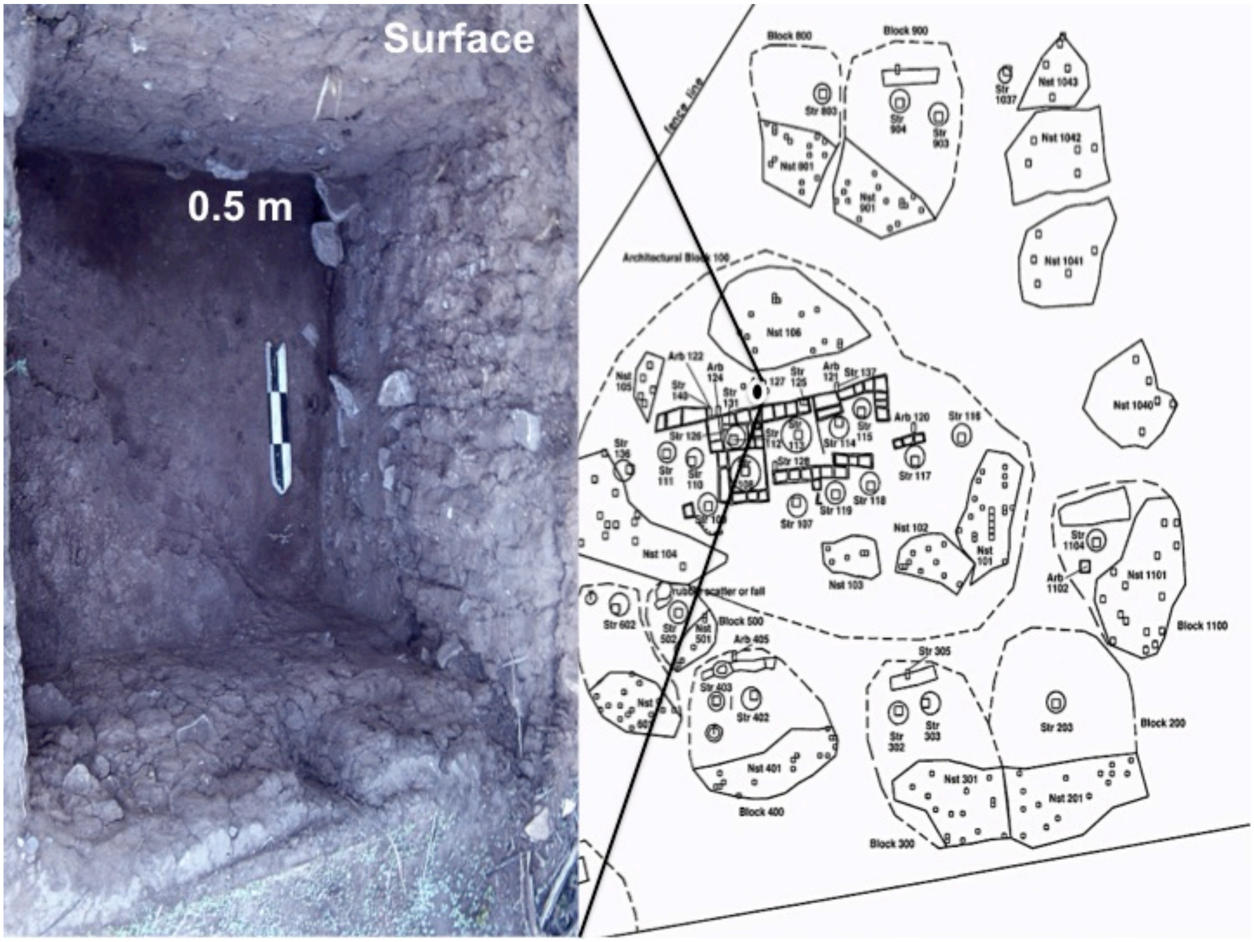

Table 6. Radiocarbon, dendrochronology, and typological ages for Albert Porter Pueblo, Colorado.

Sample	Lab #	^{14}C age yr BP	Cal age (2 σ)[a]	Probability
Bean	Beta 201369	760 ± 40	CE 1203−1294 CE 1191−1199	0.990 0.010
Maize	Beta 201368	800 ± 60	CE 1147−1293 CE 1121−1140 CE 1046−1091	0.914 0.021 0.065
Maize	Beta 201370	880 ± 40	CE 1234−1243 CE 1037−1225	0.016 0.984
Wood	Dendrochronology		CE 1110−1260	
Pueblo III Pottery			CE 1100−1250	
Pueblo II Pottery			CE 920–1140	
Basketmaker III and Pueblo I Pottery			CE 600–920	

a. CALIB 7.1 and the IntCal13 Calibration.

Figure 5. Bayesian adjustments of the radiocarbon ages using OXCAL to give the full range of possible ages for Albert Porter Pueblo, Colorado.

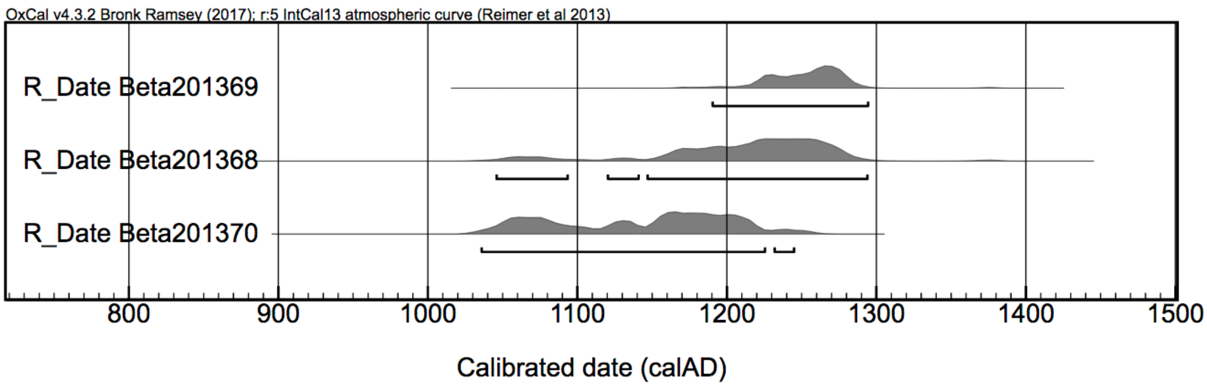

Table 7. Chronostratigraphy and Pt values for Albert Porter Pueblo, Colorado.

Depth (m)	Texture	Munsell Soil Color	Age	Pt (ppb)[a]
0.0-0.10	Loam	7.5YR4/6		1.8
0.10-0.18	Loam	7.5YR4/6		1.6
0.18-0.28	Silty Clay Loam	7.5YR5/4		5.3
0.28-0.40	Silty Clay Loam	5YR5/4	CE 1191−1294 CE 1046−1293 CE 1037−1243 CE 1110−1260 CE 1100−1250	0.7
0.40-0.50	Silty Clay Loam	5R5/4	CE 920−1140	1.4
0.50-0.55	Clay Loam	2.5YR4/6	CE 600−920	-

a. - = below detection.

Big Bone Lick, Kentucky

Big Bone Lick is located in the drainage basins of Big Bone and Gum Branch creeks, tributaries to the glaciated Lower Ohio River Valley (Figure 6)[9]. Big Bone Creek and Gum Branch are filled with late Quaternary fluvial sediments including as high-level pre-glacial deposits, two late Pleistocene terraces, and a late Holocene floodplain that is ~6 m thick. The silt-dominated alluvium extends downward from the floodplain surface with abundant wood charcoal, freshwater bivalves, gastropods, and the remains of C_3 plants, large mammals, and protohistoric to historic contact Fort Ancient, Madisonville Phase pottery (CE 1550−1700) and flaked-stone artifacts (CE 1550−1700)[9]. This stratum represents bison kill and butchering activities, which have been dated to the Little Ice Age (Table 8, Figure 7). They are overlain by a historic stratum contained early 19th century (CE 1810−1850) pottery. Natural stratigraphy was defined on the basis of soil texture and color (Table 9). Sediment samples were collected from intact stratigraphy exposed in an excavation profile wall of a natural floodplain scarp consisting of finely laminated silts and a basal clay. There was no evidence of bioturbation or other natural or cultural disturbances. The stratigraphy of the excavation discussed in this article is illustrated in Figure 6 and is described in detail elsewhere[9].

Figure 6. Profile of the Big Bone Lick, Kentucky excavation and site location.

Table 8. Radiocarbon, OSL, and typological ages for Big Bone Lick, Kentucky.

Sample	**Lab #**	**^{14}C and OSL age yr BP**	**Cal age (2 σ)[a]**	**Probability**
Euroamerican Pottery			CE 1810−1850	
Collagen (*Bison bison*)	CAMS-161264	245 ± 30	CE 1523−1559 CE 1562−1571 CE 1630−1681 CE 1739−1743 CE 1763−1802 CE 1938−1950	0.094 0.007 0.584 0.004 0.267 0.045
Collagen (*Bison bison*)	CAMS-161264	260 ± 30	CE 1519−1593 CE 1619−1670 CE 1779−1799 CE 1943−1950	0.297 0.567 0.122 0.014
Collagen (*Bison bison*)	UGa-4291	530 ± 105	CE 1272−1527 CE 1554−1633	0.909 0.091
Madisonville Pottery			CE 1550−1700	
Fort Ancient Biface			CE 1550−1700	
Quartz	UC OSL	600 ± 200	CE 1218−1618	

a. CALIB 7.1 and the IntCal13 Calibration.

Figure 7. Bayesian adjustments and the sum of the radiocarbon ages using OXCAL to give the full range of possible ages for Big Bone Lick, Kentucky.

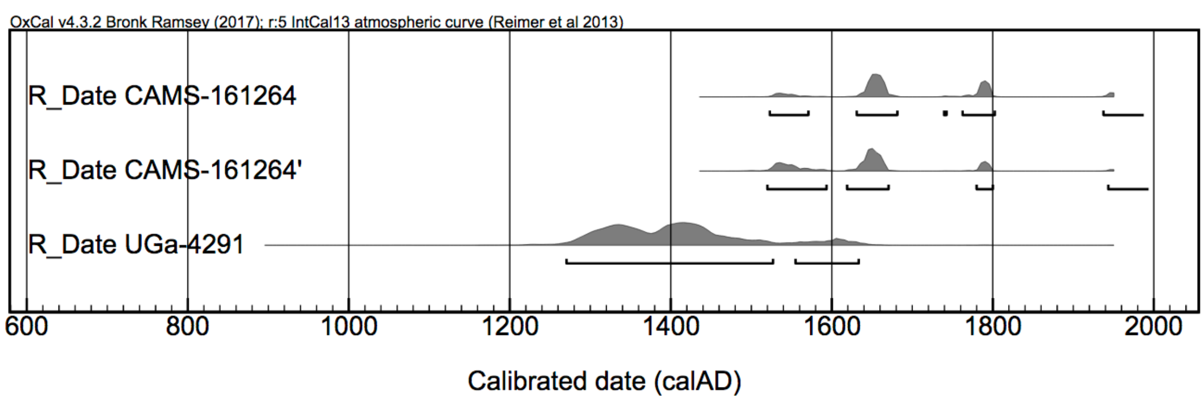

Table 9. Chronostratigraphy and Pt values for Big Bone Lick, Kentucky.

Depth (m)	**Texture**	**Munsell Soil Color**	**Age**	**Pt (ppb)[a]**
0.0-1.50	Friable Silt Clay Loam	10YR5/4		-
1.50-2.00	Silt	10YR5/6		-
2.00-2.25	Sandy Silt	10YR6/1		-
2.25-2.50	Silty Sand	7.5YR4/2		-

2.50-2.65	Sand Silt and Clay	10YR5/3-10YR7/4	CE 1810−1850	-
2.65-3.00	Clay	Gley2 4/5B	CE 1590−1799 CE 1523−1802	2.3
3.00-3.20	Sand Silt	10YR4/6	CE 1515−1700 CE 1550−1700	-
3.20-3.50	Clay	Gley2 5/10B	CE 1272−1633 CE 1218−1618	4.7

a. - = below detection.

Chaco Canyon, New Mexico

Chaco Canyon lies within the Chaco Culture National Historical Park, an UNESCO World Heritage site, located within the San Juan drainage basin of northwestern New Mexico (Figure 8). Quaternary deposits in the canyon include two late Pleistocene and early Holocene alluvial terraces and an undifferentiated late Holocene alluvial floodplain, portions of which are covered by colluvium, talus, and aeolian sand[10, 11]. While the canyon has been inhabited since the late Pleistocene, it is best known for the large number of Great Houses constructed by Ancestral Puebloans in a high elevation dry land setting. In addition to these multistory masonry pueblos and kivas, Chaco Canyon includes an extensive network of Ancestral Puebloan canals, dams, furrowed fields, gates, and reservoirs that supplied ample water to maize grown in akchin, dune, and gridded agricultural fields[12]. Sediment samples were obtained from 2 adjacent 1-m^2 excavations, which cut across an Ancestral Puebloan canal in the Chaco-Escavada Wash confluence area dated to the Pueblo II cultural period (Table 10).[10] Sediments exposed in the canal excavation document several centuries of use and modification dated using both radiocarbon and optically-stimulated luminescence (OSL) assays; canal excavations and their stratigraphy are described in detail elsewhere.[10] Little evidence of bioturbation or other types of post-depositional disturbance were evident in the canal strata. Samples were hand collected 10-cm arbitrary levels exposed in and labeled according to their stratigraphic sequence, Munsell soil color, texture (Table 11). The high platinum anomaly (43.6 ppb) at a depth of 50 to 60 cm correlates with the eruptions of the Sunset Crater volcano (Table 11)[11].

Figure 8. Profile of the Chaco Canyon, New Mexico excavation and site location.

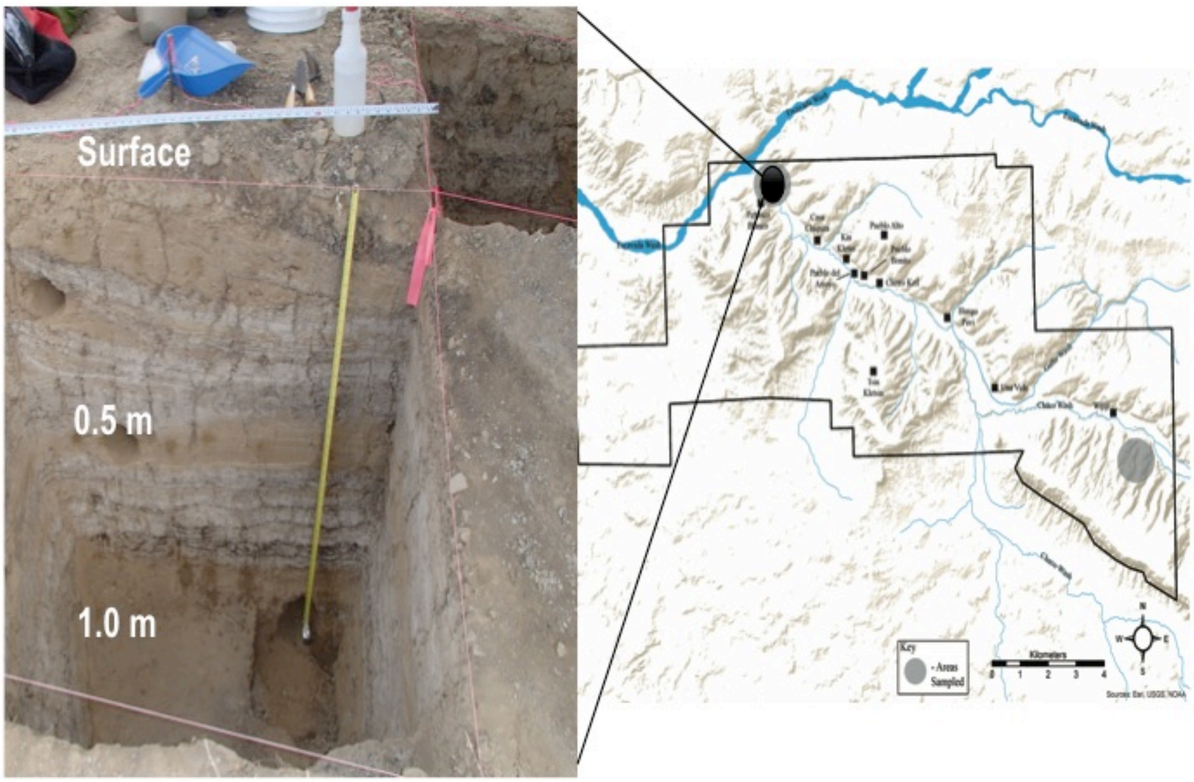

Table 10. Radiocarbon and OSL ages for the Chaco Canyon sediment samples.

Sample	**Lab #**	**^{14}C and OSL age yr BP**	**Cal Age (2 σ)[a]**	**Probability**
Wood Charcoal	UCIAMS 167243	985 ± 20	CE 997−1004 CE 1011−1049 CE 1085−1124 CE 1137−1150	0.013 0.665 0.263 0.058
Quartz	UC OSL	978 ± 60	CE 976−1096	

a. CALIB 7.1 and the IntCal13 Calibration.

Table 11. Chronostratigraphy and Pt values for Chaco Canyon, New Mexico.

Depth (m) Stratum	**Texture**	**Munsell Soil Color**	**Age**	**Pt (ppb)[a]**
0.0-0.10	Silt Sand Loam	10YR 5/3		-
0.10-0.20	Clay Loam	10YR 4/2		2.8
0.20-0.30	Fine Sand	10YR 6/4		-
0.30-0.40	Clay Loam	10YR 7/2		-
0.40-0.50	Fine Sandy Silt	10YR 6/4		-
0.50-0.60	Clay Loam	10YR 5/2	CE 997−1150 CE 976−1096	43.6

a. - = below detection.

Serpent Mound, Ohio

Serpent Mound is a >400 m long serpentine earthwork located on a karst plateau overlooking Brush Creek in southern Ohio (Figure 9)[13, 14]. Caves, sinkholes, and springs are abundant in the immediate vicinity of the earthwork. Meanders in the earthwork form the boundary of sediment-filled sinkholes, which likely held water at the time of construction. While there is some controversy over the exact age of the earthwork's construction, it overlies an early Woodland cultural component and Fort Ancient radiocarbon ages have been obtained from the earthwork berm[14]. Late Holocene sediment samples were obtained from a 3-m solid sediment core extracted from a 31 x 35 m sinkhole located ~ 100 m south of the earthwork (Table 12). The sinkhole fill represents period of intermittent ponding and drying with inclusions of Early Woodland (800−100 BCE) and Fort Ancient (CE 1000−1650) pot-sherds, flaked-stone artifacts, and abundant wood charcoal. Natural stratigraphy was defined on the basis of soil texture and color (Table 13). The stratigraphy of the core exhibited great integrity with no evidence of bioturbation or other natural or cultural disturbances (Figure 9).

Figure 9. A cross-section of the Serpent Mound, Ohio core and site location highlighting the radiocarbon sample Beta- 467476, CE 896−1021.

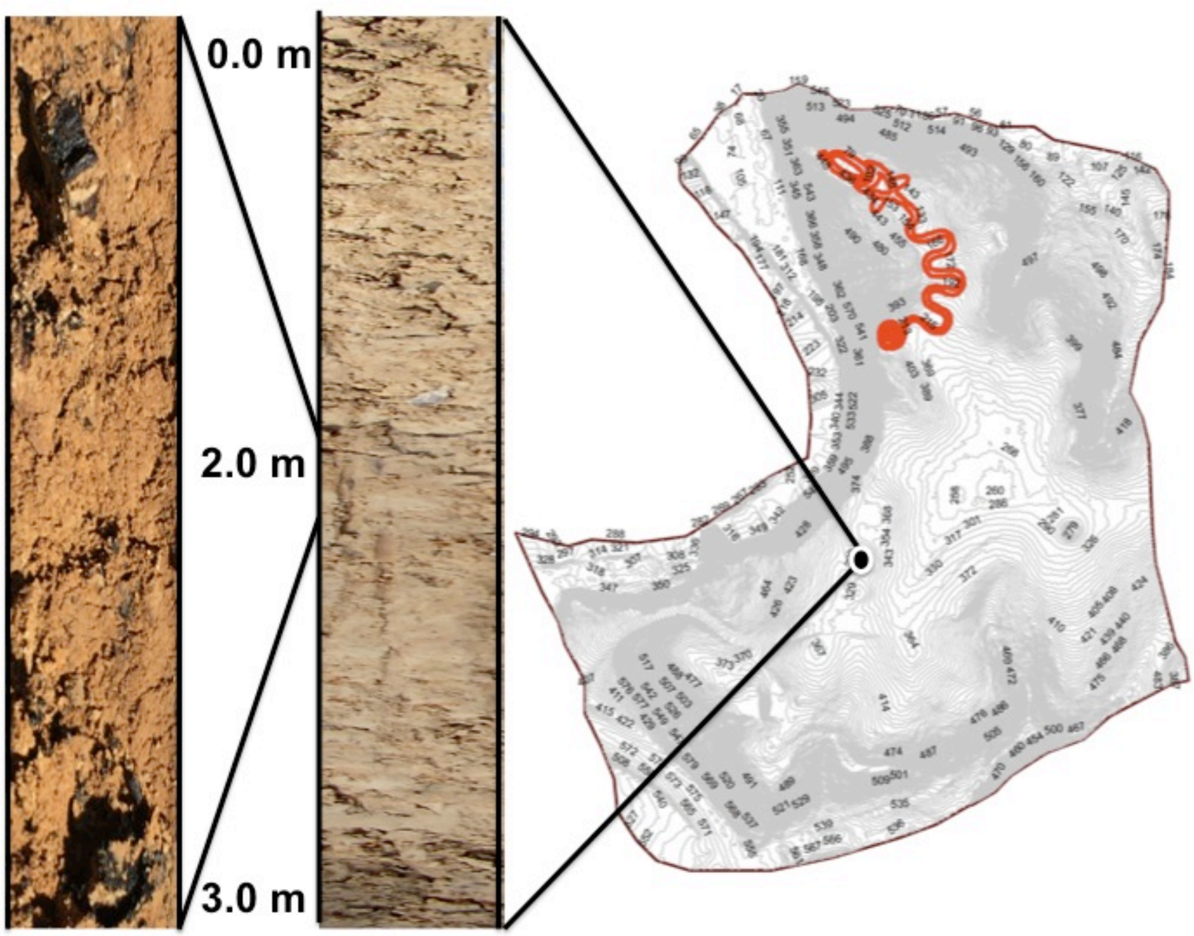

Table 12. Radiocarbon age for the Serpent Mound sinkhole.

Sample	**Lab #**	**^{14}C age yr BP**	**Cal age (2 σ)[a]**	**Probability**
Fort Ancient Pottery			CE 1000−1650	
Wood Charcoal	Beta- 467476	1070 ± 30	CE 896−927 CE 941−1021	0.215 0.785
Early Woodland Pottery			800−100 BCE	

a. CALIB 7.1 and the IntCal13 Calibration.

Table 13. Chronostratigraphy and Pt values for the Serpent Mound sinkhole.

Depth (m)	**Texture**	**Munsell Soil Color**	**Age**	**Pt (ppb)[a]**
0.0-0.10	Silt Loam	7.5YR4/4		-
0.10-0.20	Silt	7.5YR5/4		1.8
0.20-0.25	Silt Clay	7.5YR5/4		-
0.25-0.31	Clay Silt	7.5YR5/4		-
0.31-0.42	Clay Silt	7.5YR5/6		-
0.42-0.50	Silt Clay	7.5YR5/6		-
0.50-0.65	Clay Silt	7.5YR4/6		-
0.65-0.75	Silt Clay	7.5YR4/4		-
0.75-0.92	Clay Silt	7.5YR5/4		0.5
0.92-1.00	Silt Clay	7.5YR4/6		-
1.00-1.25	Clay	7.5YR5/6		1.1
1.25-1.50	Silt Clay	7.5YR6/6		-
1.50-1.62	Clay Silt	7.5YR5/6		-
1.62-1.75	Silt Clay	7.5YR4/6		0.9
1.75-2.00	Clay	7.5YR4/6	CE 1000−1650	-
2.00-2.25	Clay	7.5YR5/6	CE 896−1021	1.2
2.25-2.45	Clay	7.5YR4/4		-
2.45-2.70	Clay	7.5YR5/8		-
2.70-2.95	Stiff Clay	7.5YR5/8	800−100 BCE	-
2.95-3.09	Stiff Clay	7.5YR5/6		-

a. - = below detection.

Wallace Ruin, Colorado

Considered a “Chaco Greathouse outlier,” Wallace Ruin is an Ancestral Publoan village located in the McElmo Creek drainage basin, a tributary of the San Juan River in the Mesa Verde region of southwestern Colorado (Figure 10). The site includes Chacoan masonry, large massed buildings, blocked in kivas, an earthen berm and possible reservoir[15]. Construction phases occurred ~ CE 1040, ~ CE 1090, and ~ CE 1120 with a possible abandonment of the village in the middle of the 12th century and reuse during in the 13th century[16]. The age of Wallace ruin was determined on the basis of a detailed ceramic typology (Table 14). The pottery dates to the Pueblo II (~ CE 950–1150) and Pueblo III (~ CE 1150−1350) cultural periods[16]. Sediment samples were obtained from a solid sediment core extracted from the open plaza of the pueblo.

Natural stratigraphy was defined on the basis of soil texture and color (Table 15). The stratigraphy of the core exhibited intact stratigraphy with no signs of bioturbation or other natural or cultural disturbances (Figure 10).

Figure 10. A cross-section of the Wallace Ruin, Colorado core and site location.

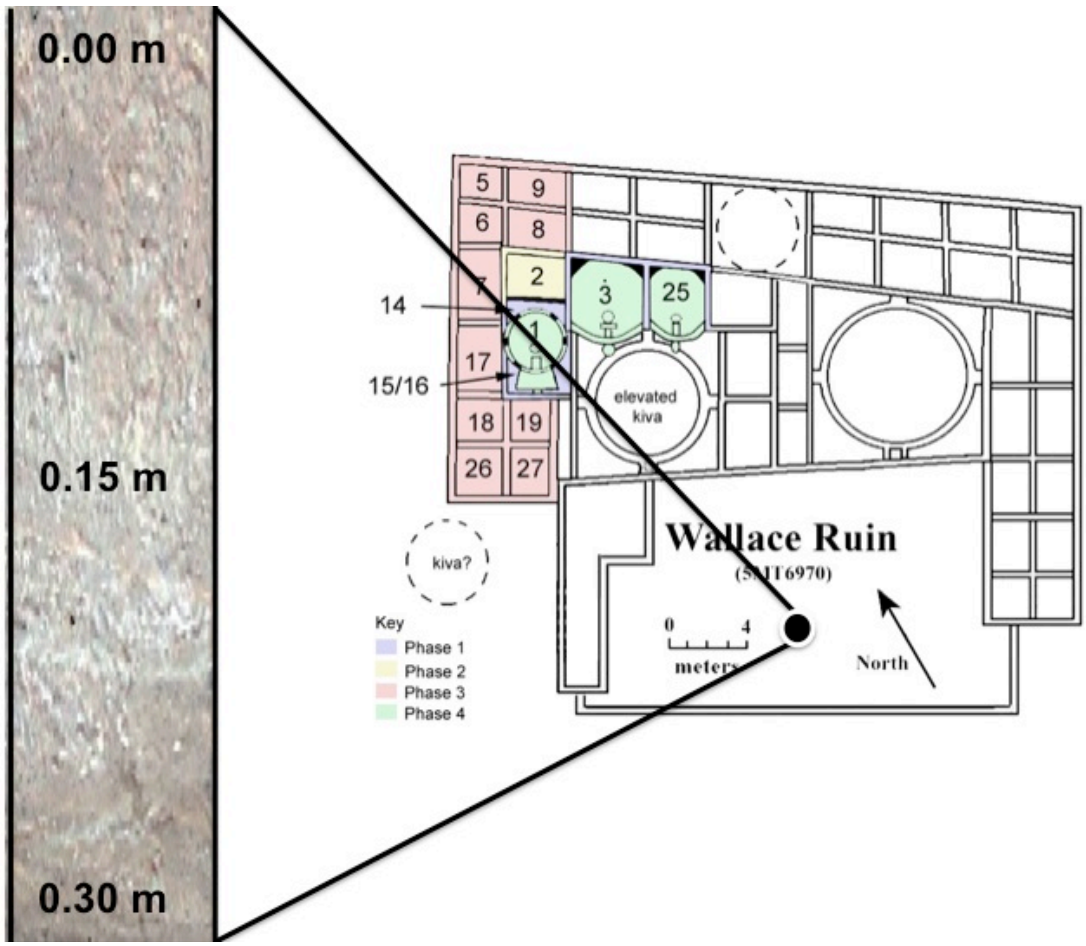

Table 14. Mean Ancestral Puebloan Ceramic ages for the Wallace Ruin, Colorado.[16]

Structure	# of Samples	Stratum	Pottery	Age
31	1	Surface	Pueblo II	CE 963
31	14	1	Pueblo II	CE 1089
31	7	3	Pueblo II	CE 1105
31	3	4	Pueblo II	CE 983
31	11	5	Pueblo II	CE 1044
31	36	Combined	Pueblo II	CE 1087

All Units	Mean	Wall Fall	Pueblo III	CE 1165
All Units	Mean	Roof Fall	Pueblo III	CE 1195
All Units	Mean	Cultural Fill	Pueblo III	CE 1168
All Units	Mean	Floor Associations	Pueblo II	CE 1145
All Units	Mean	Subfloor Not Room Associated	Pueblo II	CE 1141
All Units	Mean	Plaza Pre-room Deposits	Pueblo II	CE 1068
All Units	Mean	Wall Fall	Pueblo III	CE 1165

Table 15. Chronostratigraphy and Pt values for Wallace Ruin, Colorado.

Depth (m)	**Texture**	**Munsell Soil Color**	**Age**	**Pt (ppb)[1]**
0.0-0.10	Sand Clay Loam	7.5YR4/4		2.5
0.10-0.20	Sand Clay Loam	7.5YR3/2	CE 963−1195	-
0.20-0.32	Sand Clay Loam	7.5YR6/4	CE 936−1195	-
>0.32	Coarse-Sand Clay	5R4/4	CE 1068	-

1. - = below detection.

Wynema, Ohio, USA

The Wynema site is a stratified historic contact Fort Ancient village site located on the floodplain of the lower Little Miami River near its confluence with the Ohio River (Figure 11)[17]. The Little Miami floodplain alluvium consists of deep (~ 6 m) finely laminated calcareous silt. The village site is parallel to an abandoned late Holocene channel of the Little Miami River valley. Household features include a longhouse aligned to the summer solstice moonrise, midden deposits with historic contact Fort Ancient, Madisonville Phase (CE 1550−1700) pottery, flaked stone artifacts (CE 1550-1700) and European trade goods (~ CE 1500−1550), abundant late Holocene vertebrates, invertebrates, and carbonized plant remains. These deposits are underlain by a Middle Woodland stratum containing distinctive micro-blade cores (100 BCE−CE 500) at a depth of 1.39-3.42 m. Bison bones, ceramic typology, and an AMS radiocarbon age demonstrate that the site is contemporary with the late Holocene deposits of Big Bone Lick, Kentucky (Table 16). Sediment samples were obtained from natural stratigraphic levels exposed in a 1 x 1 excavation unit. Natural stratigraphy was defined on the basis of soil texture and color (Table

17). While rodent borrows and tree roots were exposed in the excavation, sediment samples were collected from a portion of the profile wall that showed little disturbance from bioturbation or other natural or cultural disturbances.

Figure 11. Profile of the Wynema site, Ohio excavation and site location.

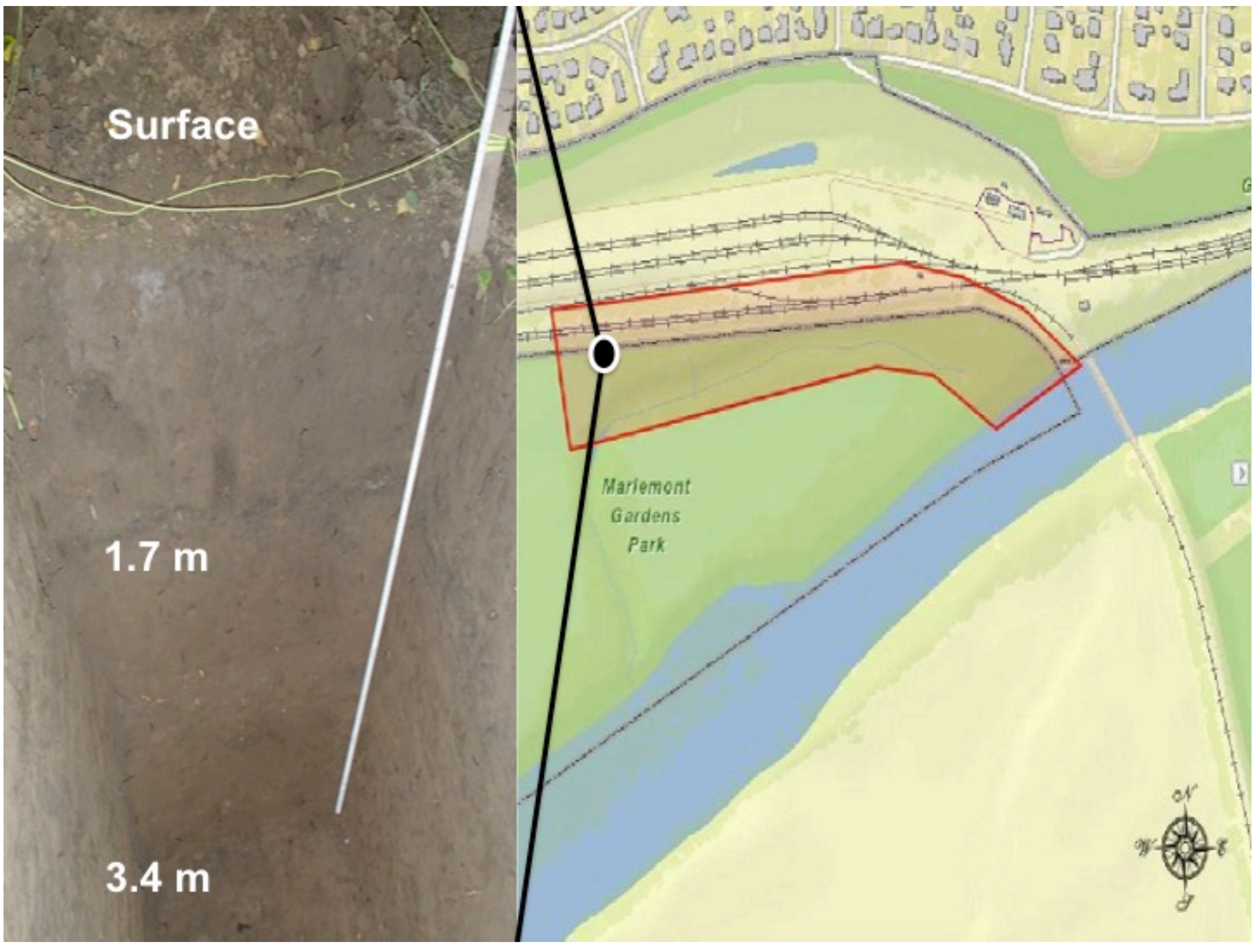

Table 16. Radiocarbon age for the Wynema site, Ohio.

Sample	**Lab #**	**^{14}C Age yr BP**	**Cal age (2 σ)[a]**	**Probability**
Madisonville Pottery			CE 1550−1700	
Fort Ancient Triangular Biface			CE 1550-1700	
Collagen (*Odocoilius viginianus*)	Beta-4291	370 ± 30	CE 1447−1527 CE 1553−1633	0.575 0.425
Hopewell Micro-blade Core			100 BCE−CE 500	

a. - = below detection.

Table 17. Chronostratigraphy and Pt values for the Wynema site, Ohio.

Depth (m)	**Texture**	**Munsell Soil Color**	**Age**	**Pt (ppb)[a]**
0.0-0.27	Silt Clay Loam	10YR5/3		2.9
0.27-0.32	Mottled Silt Clay Loam	10YR5/2	CE 1550−1700 CE 1447−1633	-
0.32-0.64	Clay Silt	10YR4/4		-
0.64-0.87	Clay Silt	10YR3/3		-
0.87-1.15	Sand Clay Silt	10YR4/3		0.6
1.15-1.39	Sand Clay	10YR4/3		1.1
1.39-3.42	Clay Silt	10YR4/3	100 BCE−CE 500	-

a. - = below detection

PT Aerosols

Three types of aerosols significantly affect the Earth's climate, volcanic, desert dust and human-made aerosols created by the burning of coal and oil. The first is the volcanic aerosol layer, which forms in the stratosphere after major volcanic eruptions like Mt. Pinatubo. The dominant aerosol layer is actually formed by sulfur dioxide gas, which is converted to droplets of sulfuric acid in the stratosphere over the course of a week to several months after the eruption[18,19]. Winds in the stratosphere spread the aerosols until they practically cover the globe. Once formed, these aerosols stay in the stratosphere for about two years. They reflect sunlight, reducing the amount of energy reaching the lower atmosphere and the Earth's surface, cooling them. The relative coolness of 1993 is thought to have been a response to the stratospheric aerosol layer that was produced by the Mt. Pinatubo eruption. In 1995, though several years had passed since the Mt. Pinatubo eruption, remnants of the layer remained in the atmosphere. Data from satellites such as the NASA Langley Stratospheric Aerosol and Gas Experiment II have enabled scientists to better understand the effects of volcanic aerosols on our atmosphere[20].

The aerosol at Erebus volcano in Antarctica is also distinct in that the gas emissions have some of the highest measured halogen/SO_2 ratios in the world as well as an abundance of heavy metals[21]. Furthermore, most of the aerosol mass appears to be narrowly confined to particles with diameter of ~0.1 mm, substantially finer than often observed at other volcanoes, which indicates it can be widely distributed by prevailing wind patterns.

Studies of volcanic aerosols from Vulcan Masaya, Nicaragua, for example, also indicate that platinum group element (PGE) concentrations (Re-Os-Ir-Rh-Ru-Pt-Pd) are significantly higher than in urban air[22]. If PGE concentrations measured in volcanic aerosols from Vulcan Masaya are typical of volcanic aerosols in general, volatile PGE emissions are globally significant and merit detailed study. The magmatic fractionation of Re-Os-Ir-Rh-Ru-Pt-Pd is governed by the volatility of relevant PGE-containing complexes (e.g., oxides, hydrogen halides, sulfides) and the physicochemical properties of the magma (temperature, fugacities of relevant chemical species). Preliminary data for volcanic aerosols from Vulcan Masaya, Nicaragua, indicate that the PGE abundance patterns are strongly and uniquely fractionated (i.e., high Pd/Pt, Os/Ir, Ru/Rh) compared to other important sources of PGE. These patterns may serve as a unique fingerprint for volcanic sources of PGEs, provided they are typical for volcanic exhalations in general. If PGE abundance patterns are a unique geochemical indicator of PGE sources in the geologic record, they may have potential applications ranging from the identification of disputed impact layers to assessing origins of PGE concentrations in the environment.

Tephra Volume

Volume determination of tephra deposits is necessary for the assessment of the dynamics and hazards of explosive volcanoes. One of the main ways volcanologists categorize the volume and explosivity of the world's major volcanic eruptions is through the analysis of tephra distribution.

This is because tephra deposits retain a large amount of important information related to the dynamics and physical parameters of the associated volcanic eruptions. One of the most important parameters that can be derived from the analysis of tephra deposits is the erupted volume, which is essential for the assessment of the associated hazards Nonetheless, the calculation of erupted volume is complicated by (1) the nonuniversal relationship of the deposit thinning with distance from the vent, (2) the poor preservation and accessibility to significant parts of tephra deposits (limited outcrops and/or tephra dispersal often over large water bodies), and (3) the difficulty in extrapolating thickness decay patterns of the medial portion of deposit, which is typically well preserved, to both proximal and distal areas. For example, the consequences of a future, caldera-forming eruption from the Yellowstone volcano have been the subject of much speculation but little quantitative research in terms of regional ashfall impacts.

Despite graphic and often fanciful media depictions of the devastation and the impact on human life that would result from a modern supereruption (producing >1000 km^3 volcanic ash or >400 km^3 dense rock equivalent of magma), no historical examples exist from which to draw comparison. The largest eruptions of the past few centuries have produced a few to several tens of cubic kilometers of magma. Examples include Tambora volcano, Indonesia in 1815, Krakatau in 1883, the Katmai/Valley of Ten Thousand Smokes eruption, Alaska in 1912, Quizapu volcano, Chile in 1932, and most recently, Pinatubo, Philippines in 1991. These erupted volumes are much larger than the Mount St. Helens eruption in 1980 (0.2–0.4 km^3), but at least an order of magnitude smaller than the largest Yellowstone events[23].

Several empirical volume calculation methods have been proposed over the past 40 years, ranging from the analysis of crystal/glass ratio of large pumices to various integration methods of thickness-versus distance- from-the-vent relations. For example, in the method described by), a sensitivity analysis was carried out on two deposits of different magnitude[24]. The determination of tephra-deposit volumes is crucial to the characterization of active volcanoes, with obvious implications for environmental and climatic impact, estimation of magma production rate, long-term hazard assessments, and forecasting of future eruptions.

For volcanic ash in the atmosphere, it is difficult to use a universal detection because the ash particle radius in the cloud usually varies from 1 to 15 μm and the chemical properties may vary from one volcano to another. The ash cloud is tracked using the brightness temperature difference for several days, but beyond that the detection is generally not reliable. Computed model results of the vertical distribution of SO_2, volcanic ash mass and particle number concentration give further insight into the atmospheric dispersion and removal processes after the eruption of Kasatochi volcano. It should be noted that the brightness temperature difference signal does not correlate with the ash content, however, comparing modeled ash column concentration with modeled data plots shows qualitative agreement in the travelling routes. Comparisons show fairly clearly that the ash cloud travelled along the same pathways as SO_2[25]. Therefore, the assumption of the same initial percentage vertical distribution for volcanic ash and SO_2 is justified for the model simulations.

References

1. Siegel, P. E., J. G. Jones, D. M. Pearsall, N. P. Dunning, P. Farrell, N. A. Duncan, J. H. Curtis, and S. K. Singh. Paleoenvironmental Evidence for First Human Colonization of the Eastern Caribbean. *Quaternary Science Reviews* 129: 275–295 (2015).

2. Jones, J. G., N. P. Dunning., N. Duncan, D. Pearsall, and P. Siegel. “Antigua.” In: Siegel,

P. (Ed.). *Island Historical Ecology: Socionatural Landscapes of the Eastern and Southern Caribbean*, Pp. 239-269. New York: Berghahn (2018).

3. Wells, E. C., S. M. Pratt, G. L. Fox, P. E. Siegel, N. P. Dunning, and A. R. Murphy. Plantation Soilscapes: Initial and Cumulative Impacts of Colonial Agriculture in Antigua, West Indies. *Environmental Archaeology* 22:23-35 (2018).

4. Dunning, N. P., R. Griffin, J. Jones, R. Terry, Z. Larsen, and C. Carr. Life on the Edge: Tikal in a Bajo Landscape. Lentz, D., N. Dunning, and V. Scarborough (eds). *Tikal: Paleoecology of an Ancient Maya City*, Pp. 95-123, Cambridge: Cambridge University Press (2015).

5. Scarborough, V., N. P. Dunning, K. Tankersley, C. Carr, E. Weaver, L. Grazioso, B. Lane, J. Jones, P. Buttles, F. Valdez, and D. Lentz. Water and Sustainable Land Use at the Ancient Tropical City of Tikal, Guatemala. *Proceedings of the National Academy of Sciences*: 12408-12413. (2012).

6. Culbert, T. P., Análisis de Cerámica. In: Proyecto de Silvacultura y Manejo de Aguas de los Antiguos Mayas de Tikal: Temporada de 2009, Lentz, D.L., Grazioso Sierra, L., Dunning, N.P., Scarborough, V.L., *Proyecto de Silvacultura y Manejo de Aguas de los Antiguos Mayas de Tikal: Temporada de 2009,* Pp. 67-75. Dirección Patrimonio Cultural y Natural de Guatemala. (2009).

7. Scarborough, V. L., L. Grazioso Sierra, N. P. Dunning, B. Lane, and E. Weaver. Manejo de Aguas en Tikal. Lentz, D.L., Grazioso Sierra, L., Dunning, N.P., Scarborough, V.L., *Proyecto de Silvacultura y Manejo de Aguas de los Antiguos Mayas de Tikal: Temporada de 2009,* Pp. 30-75. Dirección Patrimonio Cultural y Natural de Guatemala. (2009).

8. Ryan, S.C. *The Archaeology of Albert Porter Pueblo (Site 5MT123): Excavations at a Great House Community Center in Southwestern Colorado.* Crow Canyon Archaeological Center, Cortez (2015).

9. Tankersley, K.B., Murari, M.K., Crowley, B.E., Owen, L.A., Storrs, G.W., Mortensen, L. Quaternary chronostratigraphy and stable isotope paleoecology of Big Bone Lick, Kentucky, USA, *Quaternary Research* **83**, 479–487 (2015).

10. Scarborough, V.L, S. Fladd, N.P. Dunning, S. Plog, L.A. Owen, C. Carr, K.B. Tankersley, J.P McCool, A. Watson, E. Haussner, B. Crowley, K. Bishop, D. Lentz, and R. G. Vivien. Water uncertainty and ritual predictability at Chaco Canyon, New Mexico. *Antiquity*. (2018) In press.

11. Tankersley, K.B., Huff, W.D., Dunning, N.P., Owen, L.A., Scarborough, V.L. Volcanic minerals in Chaco Canyon, New Mexico and their archaeological significance. *Journal of Archaeological Science: Reports* **17**, 404-421 (2018).

12. Vivian, R.G. *The Chacoan Prehistory of the San Juan Basin*. Academic Press, New York (1990).

13. Dalby, T.S. *Geological Aspects of Key Archaeological Sites in Northern Kentucky and Southern Ohio*, Ohio Geological Survey, Columbus (2007).

14. Lepper, B., Duncan, J., Diaz-Granádos, C., & Frolking, T. Arguments for the Age of Serpent Mound. *Cambridge Archaeological Journal,* 1-18. doi:10.1017/S095977431800001X (2018).

15. Varien, M.D., Lipe, W.D., Adler, M.A., Thompson, I.M., Bradley, B.A., Southwestern

Colorado and Southeastern Utah Settlement Patterns: A.D. 1100 to 1300, Adler, M.A., (Ed.) *The Prehistoric Pueblo World, A.D. 1150-1350*, Pp. 86-113, University of Arizona Press, Tucson.

16. Bradley, B.A. *Excavations at Wallace Ruin (5MT6970) Montezuma County, Colorado 1998-2010*. University of Exeter, Exeter (2010).

17. Tankersley, K. B. and R. Newman *Dr. Charles Louis Metz and the American Indian Archaeology of the Little Miami River Valley.* Little Miami Publishing Company, Milford (2016).

18. Giammanco S, Sims, K.W.W. Neri, M.. Measurements of ^{220}Rn and ^{222}Rn and CO_2 emissions in soil and fumarole gases on Mt. Etna volcano (Italy): Implications for gas transport and shallow ground fracture. *Geochemistry, Geophysics, Geosystems*, **8**, 10:1644 (2007).

19. Villemant, B., Salaün, A., Staudacher, T., Evidence for a homogeneous primary magma at Piton de la Fournaise (La Réunion): A geochemical study of matrix glass, melt inclusions and Pélé's hairs of the 1998–2008 eruptive activity. *Journal of Volcanology and Geothermal Research* **184**, 79–92 (2009).

20. Moune, S., Faure, F., Gauthier, P.J., Sims, K.W.W., "Pele’s hairs and tears: natural probe of volcanic plume," *Journal of Volcanology and Geothermal Research*, **164**, 244-253 (2007).

21. Ilyinskaya, E., Oppenheimer, C., Mather, T.A., Martin, R.S., Kyle, P.R., Size-resolved chemical composition of aerosol emitted by Erebus volcano, Antarctica. *Geochemistry, Geophysics, Geosystems*, **11**, (3) 1-14 (2010).

22. Mills, M. J., Schmidt, A., Easter, R., Solomon, S., Kinnison, D.E., Ghan, S.J., Neely,

R.R., Marsh, D.R., Conley, A., Bardeen, C.G., Gettelman, A., Global volcanic aerosol properties derived from emissions, 1990–2014, using CESM1(WACCM), *Journal of Geophysical Research: Atmosphere*, **121**, 2332–2348 (2016).

23. Bonadonna, C., and Houghton, B.F., Total grain-size distribution and volume of tephrafall deposits. *Bulletin of Volcanology*, **67**, 441-456 (2005).

24. Christiansen, R.L and Blank, H.R. Jr., *Volcanic stratigraphy of the Quaternary rhyolite plateau in Yellowstone National Park, Wyoming*: U.S. Geol. Survey Prof. Pap. 729-B, 18 (1972).

25. Stohl, A., Prata, A.J., Eckhardt, S., Clarisse, L., Durant, A., Henne, S., Kristiansen, N.I., Minikin, A., Schumann, U., Seibert, P., Stebel, K., Thomas, H.E., Thorsteinsson, T., Tørseth, K., Weinzier, B., Determination of time- and height-resolved volcanic ash emissions and their use for quantitative ash dispersion modeling: the 2010 Eyjafjallajökull eruption, Atmospheric Chemistry and Physics, **11**, 4333–4351 (2011).